Catalysis Today 382 (2021) 120–129

Contents lists available at ScienceDirect

Catalysis Today

journal homepage: www.elsevier.com/locate/cattod

Calcination temperature effects on Pd/alumina catalysts: Particle size, surface species and activity in methane combustion

Domenica R. Fertal [a], Matteo Monai [b], Laura Proaño [c], Maxim P. Bukhovko [c], Jihyeon Park [a], Yong Ding [d], Bert M. Weckhuysen [b,*], Anil C. Banerjee [a,*]

[a] Department of Chemistry, Columbus State University, Columbus, GA 31907, United States
[b] Inorganic Chemistry and Catalysis Group, Debye Institute for Nanomaterials Science, Utrecht University, Universiteitsweg 99, 3584 CG Utrecht,The Netherlands
[c] Department of Chemical and Biomolecular Engineering, Georgia Institute of Technology, Atlanta, GA 30332, United States
[d] School of Materials Science and Engineering, Georgia Institute of Technology, Atlanta, GA 30332, United States

ARTICLE INFO

Keywords:
Pd/alumina catalysts
calcination temperature
particle size
surface species
operando DRIFTS
methane combustion

ABSTRACT

The effects of calcination temperature on Pd/γ-alumina catalysts were studied using a variety of techniques to measure particle sizes, surface species, and activity in methane combustion. Pd/Al_2O_3 catalysts were synthesized using a new impregnation-vortexing method. Three catalysts containing 3.3 wt.% Pd/Al_2O_3 were calcined at 150 °C, 250 °C, and 500 °C. The light-off temperature for methane combustion was 250-255 °C for all catalysts and 100% methane combustion was achieved at 275 °C in 20 min with the $3Pd/Al_2O_3$ 250 °C catalyst under lean methane conditions. X-ray photoelectron spectroscopy showed PdO_x and PdO on the catalysts surface, and conversion of some PdO_x to PdO and Pd^0 after reaction. Particle sizes and dispersions were different in the three fresh and spent catalysts as shown by scanning transmission electron microscopy (STEM) and CO pulse chemisorption. In situ and *operando* diffuse reflectance infrared Fourier transform spectroscopy (DRIFTS) showed that after high temperature calcination, dormant monodentate carbonates are formed at the interface of Pd and alumina on the 3 Pd/Al_2O_3 500 °C catalyst, which are absent on the $3Pd/Al_2O_3$ 250 °C catalyst during reaction. Temperature-responsive CO species were observed for both $3Pd/Al_2O_3$ catalysts, evidencing restructuring of the $3Pd/Al_2O_3$ 250 °C catalyst upon heating in accordance with the STEM results. The results indicate a varying degree of strong metal-support interactions, resulting in different adsorbed species over the catalysts during methane oxidation reaction. We suggest that, over the $3Pd/Al_2O_3$ 250 °C catalyst, the desorption of carbonates frees OH groups at the Pd-Al_2O_3 interface, which can react (with other OH or H) and desorb as water, a step which can be rate limiting on methane oxidation over Pd/Al_2O_3 at low temperatures. This research study highlights the possibility of altering catalytic properties and surfaces through calcination at different temperatures.

1. Introduction

Catalytic combustion of methane has been an important topic of research and development for more than a decade mainly due to its environmental impacts. Two reviews summarized the recent advances made in this area [1,2]. Methane combustion by palladium catalysts on alumina [3–7], ceria [8,9], and ceria-alumina [10–13] supports have been reported. To develop a better understanding of the mechanism of complete methane combustion, several researchers have worked on the effects of active Pd phases, particle size, and metal-support interactions and structure-activity relationships. Particle size, shape, chemical composition, and metal–support interaction could significantly influence the properties and activities of metal catalysts [14–16].

The role and the identity of the active phases of Pd/Al_2O_3 catalysts in methane oxidation is still not clear. Many researchers reported PdO as the active Pd species [4,6,7,17–19], while others attributed the activity to Pd^0 [20,21], as well as both Pd^0 and PdO [22,23], or PdO/PdO_x [5, 24–26]. There are also conflicting reports about the effects of particle size on methane combustion by Pd/Al_2O_3 catalysts. Stakheev et al. [27] and Murata et al. [6,28] found an increase in catalytic activity with increase in particle size. Baldwin and Burch [29] and Zou et al. [30] did not find any correlation between catalytic activity and Pd particle size.

* Corresponding authors.
E-mail addresses: b.m.weckhuysen@uu.nl (B.M. Weckhuysen), banerjee_anil@columbusstate.edu (A.C. Banerjee).

https://doi.org/10.1016/j.cattod.2021.08.005
Received 30 April 2021; Received in revised form 4 July 2021; Accepted 4 August 2021
Available online 9 August 2021

Chen et al. [7] reported monotonous decrease in activity with increase in Pd particle size due to size-dependent activity of Pd catalyst in the combustion reaction.

Preparation methods and the support could also alter the oxidation states, particle size, and surface species through metal-support interactions (MSI). The γ-Al_2O_3 support could initiate strong metal-support interactions (SMSI) with Pd nanoparticles and influence particle size and reaction mechanism during methane combustion in lean conditions [4,6,7,19,22,26,31]. There is only limited research reported on the effect of calcination temperature of Pd supported catalysts on the active phases and methane oxidation: hydroxyapatite supported palladium catalyst [32], Pd/ZrO_2 [33], $Pd/LaFeO_3$ [34], Pd/SiO_2 [35] and Pd/ZrO_2 and Pd/Al_2O_3 [36].

A new synthesis method to prepare supported Pd catalysts was developed by combining incipient wetness and vortexing methods to increase mixing and dispersion [5,13,37]. In the current study, we have improved the preparation method further and investigated the effect of calcination temperature of Pd/Al_2O_3 catalysts calcined at 150 °C, 250 °C, and 500 °C. Results showed light-off and higher methane conversion for the Pd/Al_2O_3 catalyst calcined at 250 °C, which was interpreted on the basis of structural evolution and surface intermediates observed by electron microscopy and vibrational spectroscopy. The data provided a scope for detailed investigations on the effects of calcination temperature on the active Pd phases, particle size, and surface species in the catalytic combustion of methane by Pd/Al_2O_3 catalysts under lean conditions (1:4 CH_4-O_2 ratio). The study may provide some additional insights to the mechanism of methane combustion and facilitate the future development of a more efficient Pd/Al_2O_3 catalyst for low temperature methane combustion.

2. Experimental

2.1. Catalyst and support preparation

The 3.3 wt.% Pd/ γ-Al_2O_3 (Pd/Al_2O_3) catalysts were synthesized by modifying the method described in previous work [5,37]. In the original method, the precursor palladium nitrate hydrate solution was added to the solid gamma aluminum support during vortexing. In the modified method, the catalyst was prepared by impregnating an aqueous solution of palladium nitrate hydrate (Sigma-Aldrich; $Pd(NO_3).xH_2O$, x≈2**;** formula wt. 230.43 g/mol**;** 36.4% Pd) as the precursor to an aqueous slurry of the gamma aluminum oxide (Sigma-Aldrich, 99.9%; particle size < 50 nm; surface area > 40 m^2/g) support. The precursor solution containing 0.2117 g palladium nitrate hydrate dissolved in 1.0 mL deionized water was slowly added from a syringe pump at a rate of 20 μL/min to a slurry of the support (2.0058 g gamma aluminum oxide in 5.0 mL deionized water) taken in a vortex tube. As the precursor solution was being added to the support, the mixture was simultaneously vortexed at a speed of 900 rpm in a Vortex apparatus. The addition of the entire 1.0 mL of precursor solution was complete after 1 h, followed by an additional 2 h of vortexing for intense mixing. The mixture remained in the vortex tube and was dried in an air oven at 105 °C for 12 h, ground in a mortar and pestle and then divided into three equal portions. Each portion was separately transferred to a porcelain crucible and calcined for 5 h in a muffle furnace at 150 °C, 250 °C, or 500 °C. The calcined catalysts were ground and sieved and the particles of 53-75 microns (-200 +270 ASTM sieves) sizes were used for characterization and activity experiments.

The spent catalysts were prepared by reacting the fresh catalysts with a gas mixture (1% methane, 4% oxygen, 95% nitrogen) at 220–350 °C for a total reaction time of 6 h during the catalytic activity experiments.

Two γ-Al_2O_3 references for diffuse reflectance infrared Fourier transform infrared spectroscopy (DRIFTS) experiments were prepared via the same hydrothermal treatment used for catalyst synthesis and then calcined at two different temperatures of 250 °C and 500 °C.

2.2. Catalyst characterization

2.2.1. Inductively coupled plasma optical emission spectrometry

Inductively coupled plasma optical emission spectrometry (ICP-OES) analysis of catalyst samples were performed with an Optima 8300 (Perkin Elmer, USA) instrument fitted with peristaltic pump and autosampler. The samples were digested in aqua regia (4:1 v/v HCl: HNO_3) and diluted with deionized water.

2.2.2. Pulse chemisorption

Pulse CO chemisorption was performed in Micromeritics AutoChem II 2920 (Micromeritics Corporation). The detailed methods have been described in our previous work [5,13,37] and by Sulmonetti et al. [38]. For the pulse chemisorption experiment, the catalyst was first reduced in hydrogen at 450 °C and then pulses of CO were injected. Dispersion and particle size of the catalyst were calculated from the CO uptake, wt.% of Pd loading, and assuming a 1:1 ratio between the adsorbed and Pd-active site.

2.2.3. X-ray photoelectron spectroscopy

Ex-situ X-ray photoelectron spectroscopy (XPS) analysis was performed with a Thermo K-Alpha spectrometer (ThermoFisher Scientific), using a monochromatic Al Kα radiation source. Spectra were measured in the regions of Pd 3d, O 1s, and Ce 3d. Charge referencing was performed from the C 1s region, referenced to the adventitious carbon (at 284.8 eV). The X-ray beam spot size was 400 μm and the spectrometer was operated at 50 eV pass energy and 50 ms dwell time for each step size of 0.1 eV [13].

2.2.4. Scanning transmission electron microscopy

A Hitachi HD2700 aberration-corrected scanning transmission electron microscope was used to record High-Angle Annular Dark-Field Scanning Transmission Electron Microscopy (HAADF-STEM) images, Scanning Electron Microscopy (SEM) images and Energy Dispersive Spectroscopy (EDS) mappings. The samples were prepared on a lacey carbon-coated Au grid. The electron beam convergence angle was ~27 mrad and the HAADF detector collection angle, 70–370 mrad. More details on these techniques can be found in a recent publication [39].

2.2.5. Operando diffuse reflectance infrared Fourier transform spectroscopy

Operando diffuse reflectance infrared Fourier transform spectroscopy (DRIFTS) was carried out in a Harrick high temperature DRIFTS cell, using a Bruker Tensor 37 FT-IR spectrometer equipped with a MCT detector. The catalysts powders were sieved to the 150–75 μm fraction and 10 mg of powder was loaded in the cell. The catalysts were pretreated in situ in 50 mL/min N_2 to 200 °C (ramp 10 °C/min) for 1 h at 1 bar. After pre-treatment, the methane oxidation reaction was carried out using 47.5 mL/min N_2, 0.5 mL/min CH_4, 2 mL/min O_2. The reaction gases were introduced at 200 °C for 30 min, after which the temperature was ramped to 300 °C at 5 °C/min. All gases were introduced through Bronkhorst EL-FLOW Mass Flow Controllers. During the experiments, DRIFTS spectra were collected (1 spectrum/minute) and the gas mixture coming from the cell was analyzed with an Interscience custom-built Global Analyzer Solutions (G.A.S.) Compact GC4.0 gas chromatograph that was connected to the outlet of the reaction cell, equipped with a TCD and a FID detector.

2.3. Activity experiments

The steady-state CH_4 oxidation activity was tested at constant temperatures in a 1:4 CH_4/O_2 feed for 20 min. Activity measurements were conducted in a temperature-controlled horizontal tubular fixed-bed quartz reactor (internal diameter 12 mm). The catalyst bed was heated to a desired temperature using a temperature-controlled furnace (Carbolite MTF1000). A mass of 0.1 g of a catalyst was packed in the

reactor tube with quartz wool and beads. The temperature of the catalyst bed was raised to the reaction temperature in a flow of nitrogen (150 cm^3/min). When the desired temperature was reached, the flow of nitrogen was stopped and a reacting gas mixture (1% CH_4, 4% O_2 and balance of nitrogen) was passed through the catalyst bed at a flow rate of 150 cm^3/min for 20 min. After the reaction time, a sample of 1 cm^3 of the effluent gas mix coming out of the reactor outlet was collected in a gas-tight syringe and injected into the gas chromatograph (GC Model 310, Sri Instruments, USA). The gas chromatograph was fitted with a 6 ft *shincarbon* column and a thermal conductivity detector. The concentrations of methane and carbon dioxide were measured as volume % using a *Peaksimple* software.

To repeat an activity run at a temperature, the flow of gas mixture after the first run was switched to nitrogen gas while maintaining the original temperature. After 20 min, the flow of the gas was changed to the reacting gas mixture (1% CH_4, 4% O_2 and balance of nitrogen) and the second run was conducted for 20 min. For each activity experiment at a temperature, three consecutive runs were taken to check reproducibility and only methane conversion values within 2-3% error were accepted. For each activity run, a gas hourly space velocity (GHSV) of 90,000 (cm^3/g catalyst at 25 °C and 1.0 atm) hr^{-1} and reaction time of 20 min were used. The 20-min reaction time was chosen to reach steady state reaction conditions in the catalyst bed. The concentration of methane (vol %) was calculated from a calibration curve of methane peak area obtained from the GC and vol % methane in three standard gas mixtures containing 1%, 2% and 4% methane. The methane conversion (% v/v) was calculated from the volume % of methane in the gas mixture before and after the reaction.

3. Results and discussion

3.1. Catalyst composition and designation

We chose high Pd loadings (3.3 wt%) for the characterization of the Pd active phases by XPS, particle sizes/shapes by STEM, and surface species by *operando* DRIFTS. We have used palladium nitrate hydrate as Pd precursor since it has a low decomposition temperature (~100 °C). We have prepared catalysts by calcining at 150 °C, 250 °C, and 500 °C to study the effect of calcination on the catalyst structure, surface chemistry, and performance in methane oxidation. Since the Pd precursor is hygroscopic and it contains an undefined amount of water of hydration, we have used ICP-OES analysis to determine the final Pd wt. % in the catalyst samples. The Pd elemental content of 3.3 wt.% Pd was close to the calculated value of 3.7 wt% Pd. For simplicity, the catalysts synthesized based on the Pd wt.% and calcination temperature are designated as follows in this paper: 3 Pd/Al_2O_3 150 °C for 3.3 wt.% Pd calcined at 150 °C; $3Pd/Al_2O_3$ 250 °C for 3.3 wt.% Pd calcined at 250 °C; and $3Pd/Al_2O_3$ 500 °C for 3.3 wt.% Pd calcined at 500 °C. We also used the terms “Fresh” and “Spent” to designate the original catalysts and the catalysts after methane combustion.

A comparison of the catalyst ($5Pd/Al_2O_3$ calcined at 500 °C) reported in our previous publication [37] with the $3Pd/Al_2O_3$ 500 °C catalyst synthesized in the current study shows significant improvements in properties and methane activities for the $3Pd/Al_2O_3$ 500 °C. It appears that the addition of the precursor solution to a slurry of the alumina support instead of addition of the precursor solution to the solid support [5,37] improved mixing and dispersion. The results indicate that preparation methods could alter catalytic properties [1,2,5,13,37].

3.2. Effect of calcination temperature on particle size

Morphology (shapes and sizes of Pd particles) of the fresh and spent catalysts ($3Pd/Al_2O_3$ 150 °C, 3 Pd/Al_2O_3 250 °C, and 3 Pd/Al_2O_3 500 °C) were estimated from the HAADF-STEM and SEM images (Figs. 1–3), and the corresponding nanoparticles (NPs) size distribution histograms are shown in Fig. 4. All catalysts showed a rather broad nanoparticle size distribution (3–10 nm), with the exception of the fresh 3 Pd/Al_2O_3 250 °C, on which a bimodal NPs size distribution was observed, with a large number of small Pd/PdO_x nanoparticles (1-3 nm) in combination with the bigger NPs observed on the other catalysts. Such small NPs showed low thermal stability, since they are not observed on the spent $3d/Al_2O_3$ 250 °C catalyst and on the $3Pd/Al_2O_3$ 500 °C catalysts. The absence of small NPs in the case of the $3Pd/Al_2O_3$ 150 °C catalyst suggests that smaller particles are formed due to metal-support interactions favoring Pd redistribution.

HAADF STEM images show that the 5-10 nm PdO/PdO_x particles are polycrystalline and corrugated, with domains showing approximate planar distances of 2.1–2.6 Å, corresponding to PdO (101), 2.1 Å

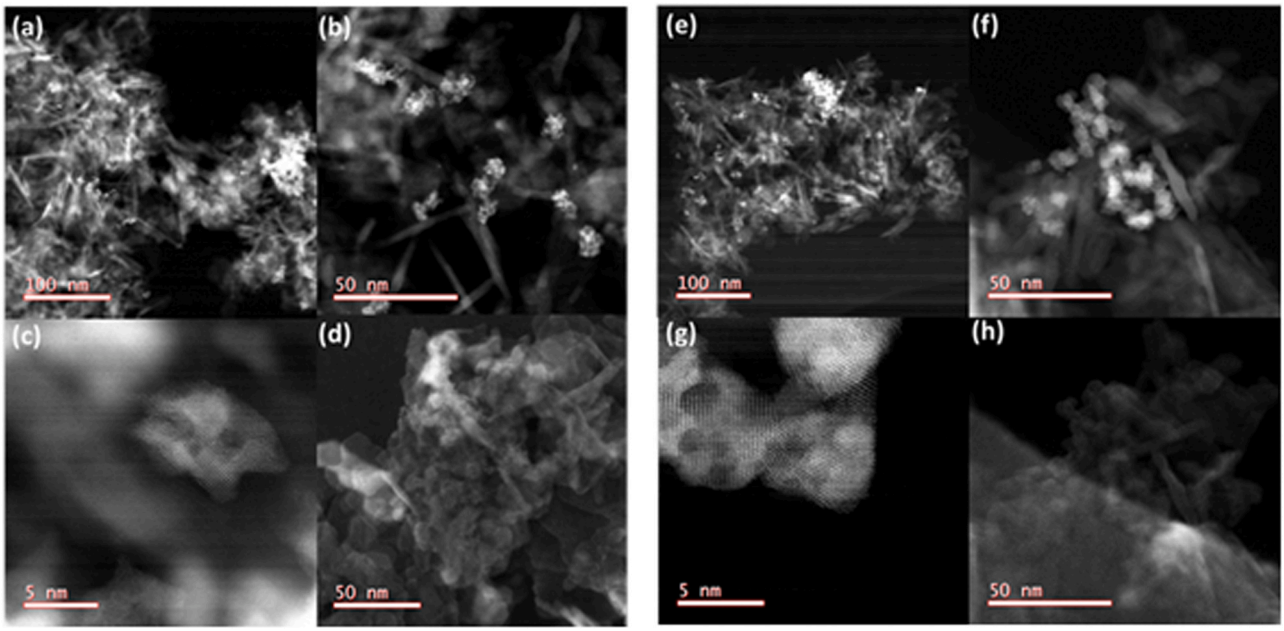

Fig. 1. HAADF STEM images in different magnifications of fresh (a, b, c) and spent (e, f, g) catalyst 3 Pd/Al_2O_3 150 °C; (d) and (h) SEM images from the same area as displayed in (b) and (f).

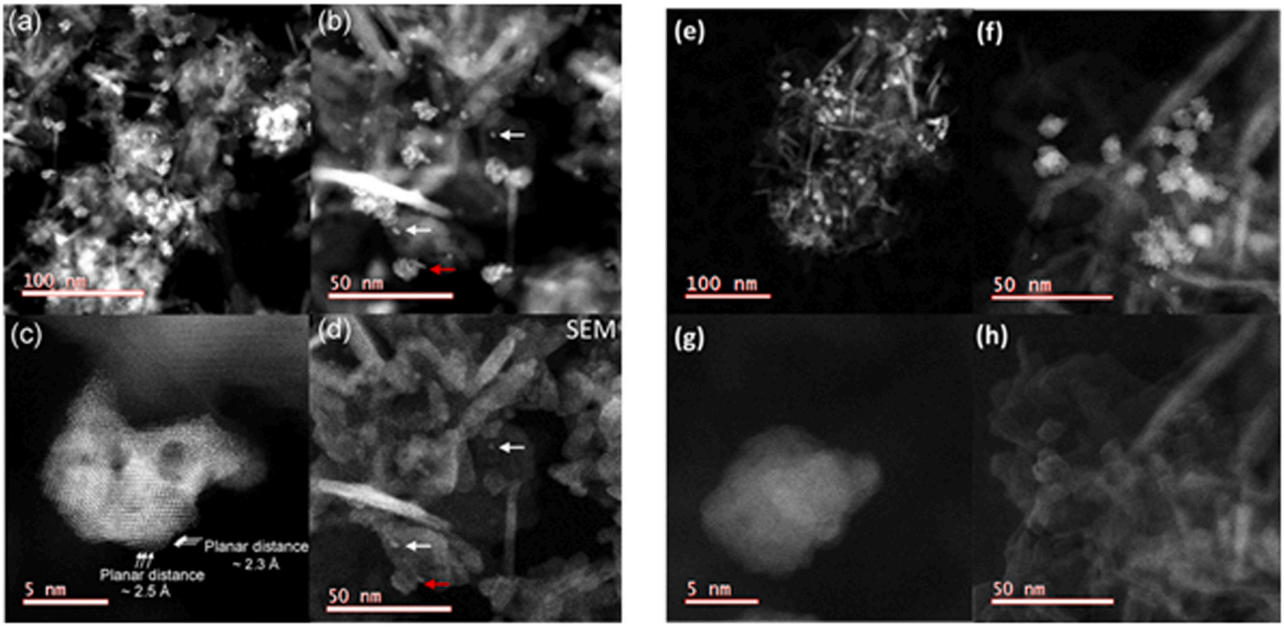

Fig. 2. HAADF STEM images in different magnifications of fresh (a, b, c) and spent (e, f, g) 3Pd/Al_2O_3 250 °C catalyst; (d) and (h) gives the SEM images from the same area as displayed in (b) and (f); the white and red arrow heads in (b) and (d) marked out the small Pd particles and large Pd clusters respectively in both HAADF and SEM images; (c) shows the approximate planar distance in the crystal lattice of PdO/PdOx.

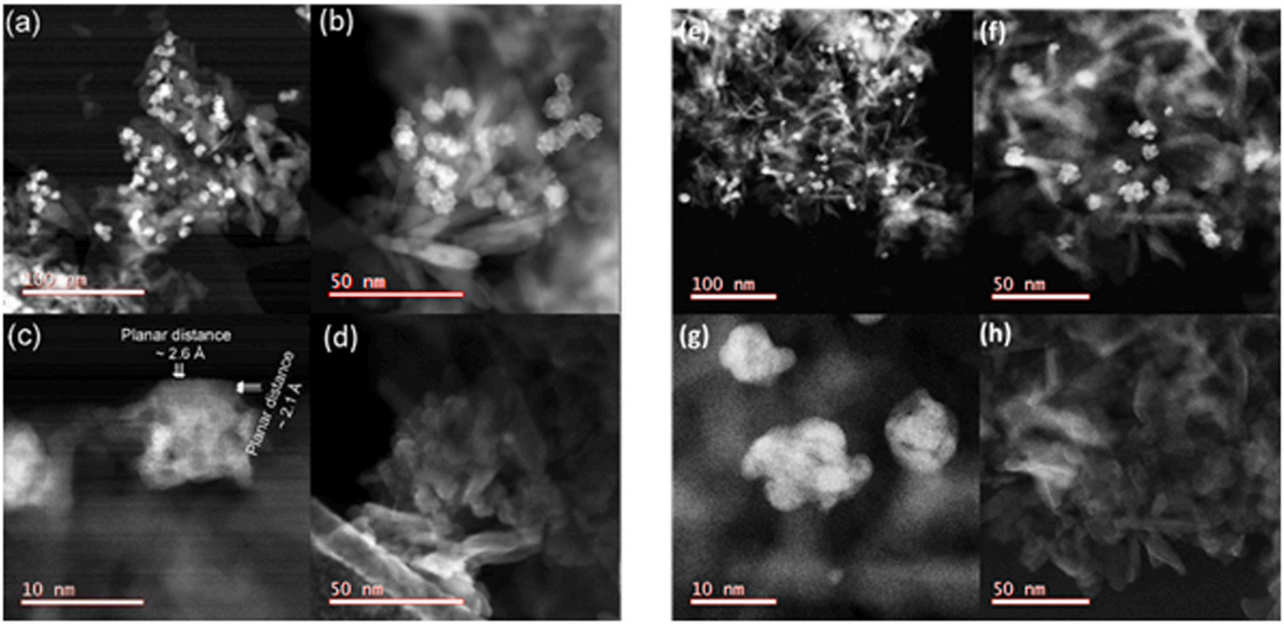

Fig. 3. HAADF STEM images in different magnifications of fresh (a, b, c) and spent (e, f, g) catalyst 3Pd/Al_2O_3 500 °C; (d) and (h) SEM images from the same area as displayed in (b) and (f); (c) shows the approximate planar distance in the crystal lattice.

assigned to PdO (110) and 2.3 Å corresponding to Pd (111). The presence of both PdO and Pd is also confirmed by XPS results (vide infra).

To complement the HAADF-STEM and SEM results, we have performed CO chemisorption experiments on both the fresh and spent catalysts, as summarized in Table 1. In agreement with STEM results, the fresh 3Pd/Al_2O_3 250 °C catalyst showed the highest dispersion, which decreased after reaction due to particle growth, reaching a final exposed metal area comparable to the spent 3Pd/Al_2O_3 500 °C. Interestingly, the dispersion of the 3Pd/Al_2O_3 500 °C increased during reaction, suggesting restructuring of the polycrystalline NPs. Comparison of the STEM images of the fresh and spent catalysts in Fig. 3 shows the presence of some small particles in the spent catalyst calcined at 500 C and this supports pulse chemisorption data in Table 1. On the other hand, CO chemisorption was hampered on the 3 Pd/Al_2O_3 150 °C catalyst, resulting in an apparent dispersion of 11% in the fresh catalyst (9 nm NPs) to almost zero in the spent catalyst. Since STEM results indicate that the NPs size is comparable on the three spent catalysts, such a low value suggests the presence of agglomerates in the catalyst which were not evidenced by local images.

A remarkable effect of calcination temperature in this research study is the change in particle sizes and the effect on particle restructuring during methane combustion. Transmission electron microscopy (TEM)

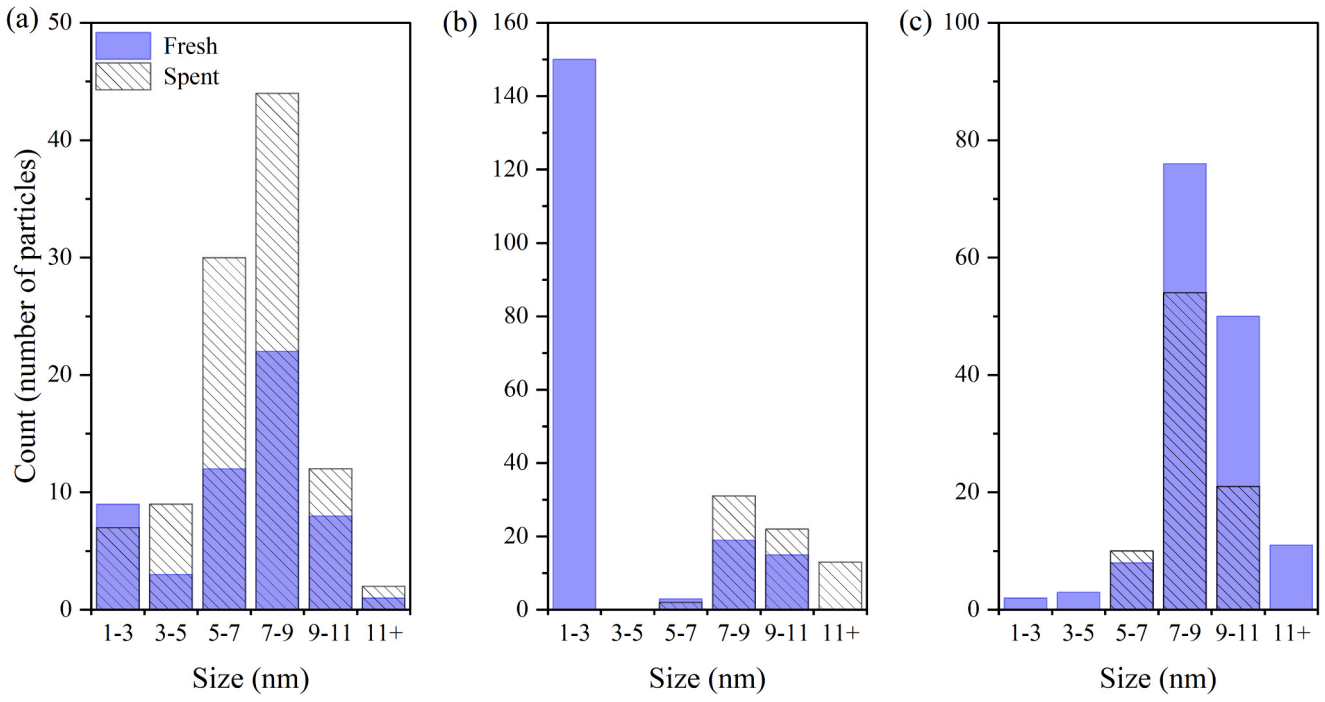

Fig. 4. Particle size distribution in fresh and spent (a) 3Pd/Al_2O_3 150 °C, (b) 3Pd/Al_2O_3 250 °C and (c) 3Pd/Al_2O_3 500 °C catalysts.

Table 1
Properties of the catalysts under study.

Properties	Values					
	3 Pd/Al_2O_3 150 °C		3 Pd/Al_2O_3 250 °C		3 Pd/Al_2O_3 500 °C	
	Fresh	Spent	Fresh	Spent	Fresh	Spent
CO uptake in chemisorption (μmol/g)	36.8	2.7	102.1	68.3	17.3	55.44
Dispersion (%)	11.9	0.88	32.9	22.01	5.6	17.87
Metal Surface Area (m^2/g)	1.7	0.13	4.8	3.2	0.8	2.6
Nanoparticle diameter (hemisphere) (nm)	9.4	127.8	2.8	4.2	16.8	6.26

images of Pd/hydroxyapatite support showed quasi-spherical Pd particles of 4–12 nm sizes for the catalyst calcined at 500 °C and progressive in particle sizes with increase in the calcination temperatures [32]. Pd/ZrO_2 calcined at 500 °C generated small and/or non-crystalline PdO clusters and the sizes increased to 10–100 nm when calcined at 1100 °C [33]. Similar trends were also observed with Pd/$LaFeO_3$ catalysts showing increase in particle sizes with increase in the calcination temperature in the range 300–700 °C [34]. We did not find any reported research on the effect of calcination temperature on Pd particle sizes in Pd/Al_2O_3 catalysts. The presence of small Pd particles (1–3 nm) on the support surface in the 3 Pd/Al_2O_3 250 °C catalyst indicates strong metal-support interactions between PdOx/PdO and Al_2O_3 support [5–7, 13,40,41].

3.3. Effect of calcination temperature on active phases

To elucidate the effect of calcination temperature on the degree of oxidation of the Pd/PdO_x active phase, we performed XPS analysis of the fresh and spent catalysts. Table 2 gives the atomic % of Pd, PdO and PdO_x based on deconvolutions of $3d_{5/2}$ peak in the Pd 3d XPS spectra. Fig. 5 shows the deconvolution of the $3d_{5/2}$ peak in the Pd 3d spectrum. Based on previously reported studies [42–44], the $3d_{5/2}$ peak in the Pd 3d spectrum was deconvoluted into 3 peaks at 335.1, 336.5, and 338 eV to determine the percentage of Pd^0, PdO (or Pd^{2+}), and PdO_x (where x > 1 or $Pd^{\delta+}$ where δ > 2) species, respectively. Peak deconvolution was performed using Avantage Data Software (Thermo Fisher Scientific) by fixing the Pd 3d peak binding energies after adjusting for charge shift using 284.8 eV as the binding energy for adventitious carbon. The 3Pd/Al_2O_3 calcined at 150 °C and 250 °C had less Pd^0 content and higher oxidation state Pd species ($Pd^{\delta+}$) (Table 2). All three catalysts contain substantially more PdO compared to Pd^0 and PdOx; however, the 3Pd/Al_2O_3 250 °C catalyst has more PdO_x.

Table 2
Atomic % of Pd, PdO and PdOx based on deconvolutions of $3d_{5/2}$ peak in the Pd 3d XPS spectra.

Catalyst		Pd^0 (at.%)	PdO (at.%)	PdO_x (at.%)
3Pd/Al_2O_3 150 °C	Fresh	4.6	76.7	18.7
	–	–	–	–
3Pd/Al_2O_3 250 °C	Fresh	4.2	68.9	26.8
	post reaction	*20.7*	*70.1*	*9.2*
3Pd/Al_2O_3 500 °C	Fresh	9.9	72.2	17.9
	post reaction	*18.8*	*70.6*	*10.6*

The data in Table 2 also reveals the change in atomic % of Pd species after methane combustion. While the atomic % of PdO remains almost constant, the change in PdO_x to Pd^0 is relatively higher in the 3 Pd/Al_2O_3 250 °C catalyst. Both spent 250 °C and 500 °C calcined catalysts show more Pd metal species (and less PdOx), suggesting possible reduction of PdO_x to Pd^0 during reaction [23]. Accordingly, PdO is the thermodynamically most stable phase in the presence of 2-4% oxygen in the temperature range 300–600 °C, but the thermodynamically stable fraction of Pd increases with temperature [17].

As stated in the introduction, the issue of active phase/s (Pd^0, PdO, PdOx) of Pd catalysts in methane combustion is still unsettled [4,5,17, 24–26,45]. Additionally, there is only limited research reported in the literature on the effect of calcination temperature on active Pd phases in supported Pd catalysts. XPS of a Pd catalyst on hydroxyapatite-support calcined at 500 °C showed higher Pd^0 percent and conversion of Pd^0 to more PdO as the calcination temperature was increased to 700 °C [32].

Domingos et al. [36] synthesized a Pd/Al_2O_3 catalyst by

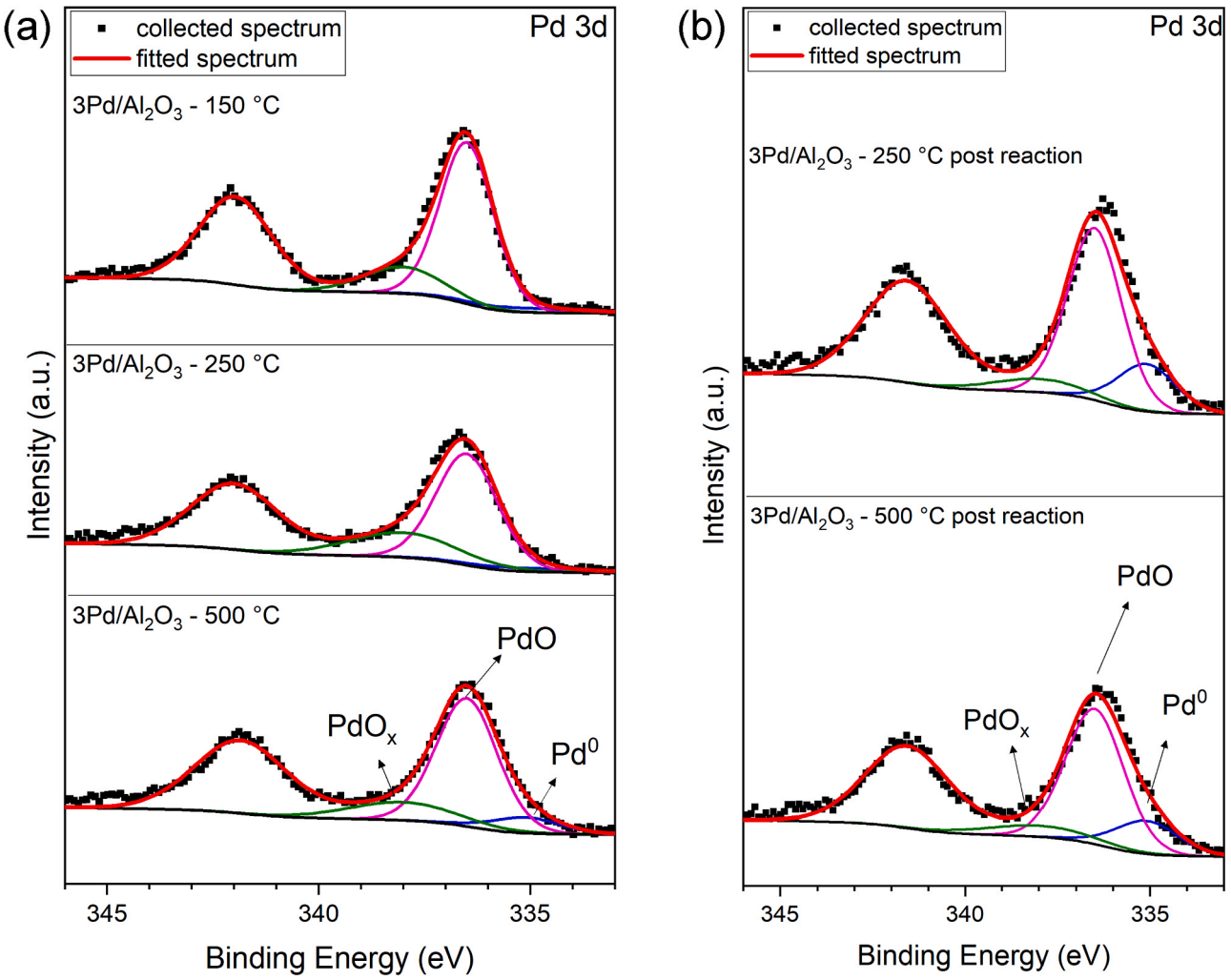

Fig. 5. The Pd 3d region of XPS spectra and fitting of the Pd $3d_{5/2}$ peak for the fresh (a) and spent (b) Pd/Al_2O_3 catalysts calcined at three temperatures.

impregnation method and calcined at 600 °C and 1000 °C. XPS data showed PdO_x as the predominant species on the surface at 600 °C and decrease in PdO_x % at a higher calcination temperature of 1000 °C. Schmal et al. [46] detected PdO/PdO_x and no Pd^0 at the surface of Pd/Al_2O_3 catalysts. Our results showing PdO and PdO_x as the predominant phases are also similar to those reported by some researchers [5, 24–26,36,47]. However, in our research we observed the effect of calcination temperature at a much lower temperature range (150–500 °C) compared to those reported in previous studies.

3.4. *Effect of calcination temperature on catalytic activity*

The % methane combustion for the $3Pd/Al_2O_3$ catalysts calcined at 150 °C, 250 °C, and 500 °C are given in Fig. 6. The methane conversion was higher with the 3 Pd/Al_2O_3 150 °C catalyst at 230–250 °C. However, the conversion was lower for this catalyst at 275–300 °C compared to the activity of the two catalysts calcined at 250 °C and 500 °C. This is consistent with the observed reduced CO chemisorption observed for the spent $3Pd/Al_2O_3$ 150 °C catalyst. The light off temperature was 250–255 °C for both 3 Pd/Al_2O_3 250 °C and $3Pd/Al_2O_3$ 500 °C catalysts. Another important feature was the complete combustion of methane (100%) at 275 °C with the 3 Pd/Al_2O_3 250 °C catalyst compared to 73% and 82% methane conversions with the catalysts calcined at 150 °C and 500 °C. The lower light-off temperature and higher conversion with the Pd/Al_2O_3 250 °C catalyst could be ascribed to a higher metal dispersion (Table 1) and a higher percentage of PdO_x on the surface of the catalyst (Table 2). This also suggests that PdO_x was the active phase of $Pd/\gamma\text{-}Al_2O_3$ catalysts in the methane combustion at temperatures below 300 °C [5,13,24–26,36,37,46]. Similar trends of decrease in the catalytic activity with increasing calcination temperature were also observed with $Pd/\gamma\text{-}Al_2O_3$ [36] and $Pd/LaFeO_3$ [34] catalysts.

The apparent activation energies for methane combustion with the three Pd/Al_2O_3 catalysts calcined at 150 °C, 250 °C and 500 °C were calculated from the Arrhenius plots derived from activity experiments conducted in the kinetic regions at 230–245 °C corresponding to methane conversion below 25%. The results are shown in Fig. 7. The lower activation energy of the $3Pd/Al_2O_3$ 150 °C catalyst is in accordance with the better activity of this catalyst at lower reaction temperatures. The catalyst, however, performed worse than the others after 250 °C. This can be rationalized based on the pulse CO chemisorption results of the spent $3Pd/Al_2O_3$ 150 °C catalyst, which indicated that PdO/PdO_x particles on the 150 °C catalysts sinter during the reaction. On the other hand, the activation energies for the $3Pd/Al_2O_3$ 250 °C and $3Pd/Al_2O_3$ 500 °C catalysts are comparable keeping in view the experimental errors in computing activities at low temperatures. The results are in accordance with the similar light-off activity at lower reaction temperatures. To explain their different activity at temperatures higher than 250 °C, we performed *operando* DRIFTS experiments to gain further insights into surface species formed during reaction (*vide infra*).

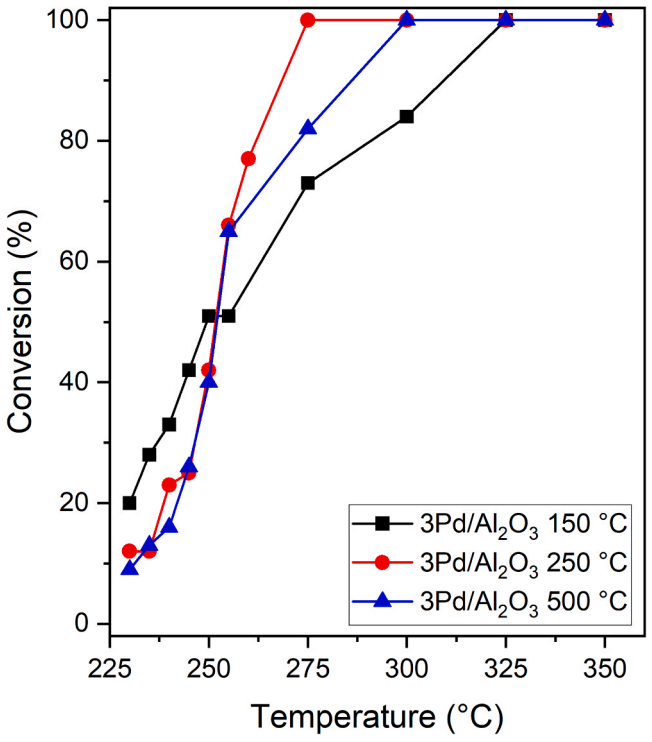

Fig. 6. Effect of calcination temperature on methane conversion. Reaction time, 20 min; GHSV, 90,000 (cc/g.cat)/ h; particle size, 53–75 microns.

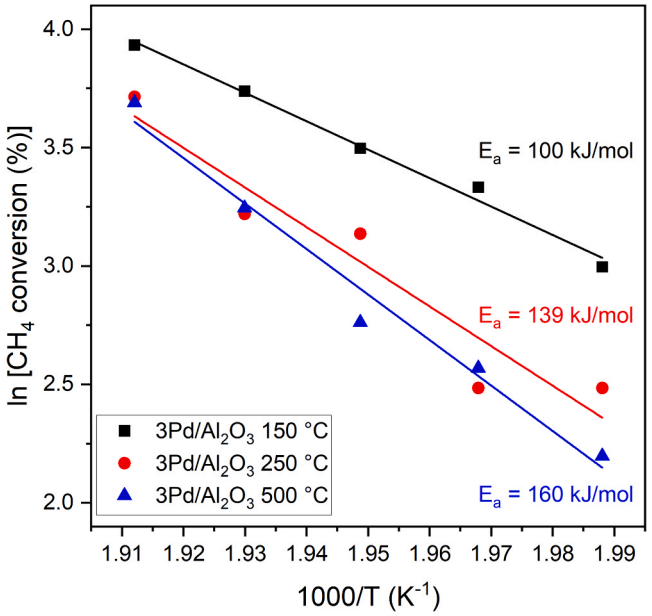

Fig. 7. Arrhenius plots for the calculation of apparent activation energy of methane oxidation over the Pd/Al_2O_3 catalysts calcined at three temperatures. Reaction conditions: Reaction time, 20 min; GHSV, 90,000 (cc/g.cat)/ h; particle size, 53–75 μm.

3.5. *Effect of calcination temperature on surface species*

To gain further insights into the surface chemistry of the studied catalysts, in situ and *operando* DRIFTS experiments were performed during the catalyst pretreatment (degassing in N_2) and methane oxidation reaction. Fig. 8A shows the evolution of H_2O- and CO_2-related species formed upon exposure to air, during degassing in N_2 to 200 °C, for the $3Pd/Al_2O_3$ 500 °C (solid lines) and γ-Al_2O_3 calcined at 500 °C (dashed lines). After high temperature calcination and exposure to air, carboxylate species and monodentate carbonate are formed on $3Pd/Al_2O_3$ 500 °C, as shown by the typical vibrations at 1635 and 1425 cm^{-1} (carboxylate, CO_2^-, ν_s and ν_{as}, respectively) and at 1530 and 1305 cm^{-1} (carbonate monodentate, COO^-, ν_s and ν_{as}, respectively) [48]. The observed carboxylate species evolve during N_2 pretreatment converting into carbonate monodentate species at 200 °C (Fig. 8A). Notably, these species are not observed on γ-Al_2O_3 calcined at 500 °C (Fig. 8A, dashed line), and similarly are absent on γ-Al_2O_3 calcined at 250 °C and on $3Pd/Al_2O_3$ 250 °C (not shown, comparable to 500 °C pretreated γ-Al_2O_3). This indicates that monodentate carbonate species are formed only in the presence of Pd, and only after high temperature treatment. This can be ascribed to a lower OH group population on alumina treated at high temperature [49], which favors adsorption of carbonates and may influence the catalytic activity of the $3Pd/Al_2O_3$ catalyst by a change in the species adsorbed at the metal-support interface, possibly explaining the difference in activity at higher temperature (Fig. 6).

To get further information about species formed during catalysis, we ran *operando* DRIFTS under methane oxidation conditions in the temperature range 200–300 °C on $3Pd/Al_2O_3$ 250 °C and $3Pd/Al_2O_3$ 500 °C catalysts (Fig. 8B and 9C, respectively), using the pure γ-Al_2O_3 calcined at 250 and 500 °C as reference (dashed lines) to pinpoint the species which are due to the presence of Pd/PdO_x. Distinct CO adsorbate species are observed only in the presence of Pd, respectively for 250 °C and 500 °C pretreated samples: a weak band at ca. 2060 and 2052 cm^{-1} (linearly bound, CO_{top} on Pd), a more intense band at ca. 1958 cm^{-1} (only for 250 °C) previously ascribed to bridge bonded μ_2-CO on Pd (100) plane [50–51] and a band at ca. 1930 or 1911–1924 cm^{-1} ascribed to μ_3-CO adsorbed on hollow sites on Pd(111) planes (Fig. 8D, solid lines) [50]. On $3Pd/Al_2O_3$ 250 °C, the 1958 cm^{-1} band disappears with increasing temperature, suggesting a restructuring of the Pd NPs during reaction and a transformation of μ_2-CO species to μ_3-CO. This is in accordance with the NPs evolution observed in STEM (Fig. 2) and CO chemisorption (Table 1)

On the $3Pd/Al_2O_3$ 500 °C catalyst, on the other hand, mainly μ_3-CO species are observed at 200 °C together with CO_{top} species with signals slightly increasing in intensity and shifting to higher wavenumbers with temperature (Fig. 8D, dashed lines). These trends suggest that the Pd surface becomes more covered with CO with higher temperature, which may be ascribed to a stronger interaction of CO with the Pd surface, resulting in partial poisoning, as indicated by the lower wavenumbers with respect to $3Pd/Al_2O_3$ 250 °C. This in turn is also consistent with the lower intrinsic activity observed after 500 °C calcination (Fig. 6).

The position (wavenumbers) of the observed CO signals are consistent with previously reported CO adsorption experiments at similar temperatures over Pd/Al_2O_3 catalysts [50]. The position of the signal is indeed temperature-dependent, with hypsochromic shifts of 30-60 cm^{-1} observed with higher temperature due to coverage effects [50,52]. Interestingly, no bands relative to CO adsorbed on Pd oxides (2110–2150 cm^{-1}) were observed [52], which suggests either that (i) the surface of Pd is completely reduced, or that (ii) CO adsorbed on PdO_x is too reactive to be observed, *i.e.* not involved in the rate-determining step. Since XPS results suggest that PdO_x is present on the surface of the catalyst (Fig. 5), hypothesis (ii) is in better agreement with our results. Accordingly, a linear correlation was previously found between the CH_4 oxidation activity of $Pd(-Pt)/Al_2O_3$ catalysts and the amount of CO_{top} adsorbed on PdO_x at 40 °C [52], indicating PdO_x is an active species in the reaction.

Notably, the monodentate carbonate species on $3Pd/Al_2O_3$ 500 °C are mostly dormant, since they do not evolve under reaction conditions, and are only slightly decreasing in intensity upon heating to 300 °C (Fig. 8C). On the other hand, carbonates are not observed on $3Pd/Al_2O_3$ 250 °C or the pure alumina supports (Fig. 8B, and dashed lines in Fig. 8C), indicating that this is a specific interfacial effect only present on the 3 Pd/Al_2O_3 500 °C catalyst. The results may be used to rationalize

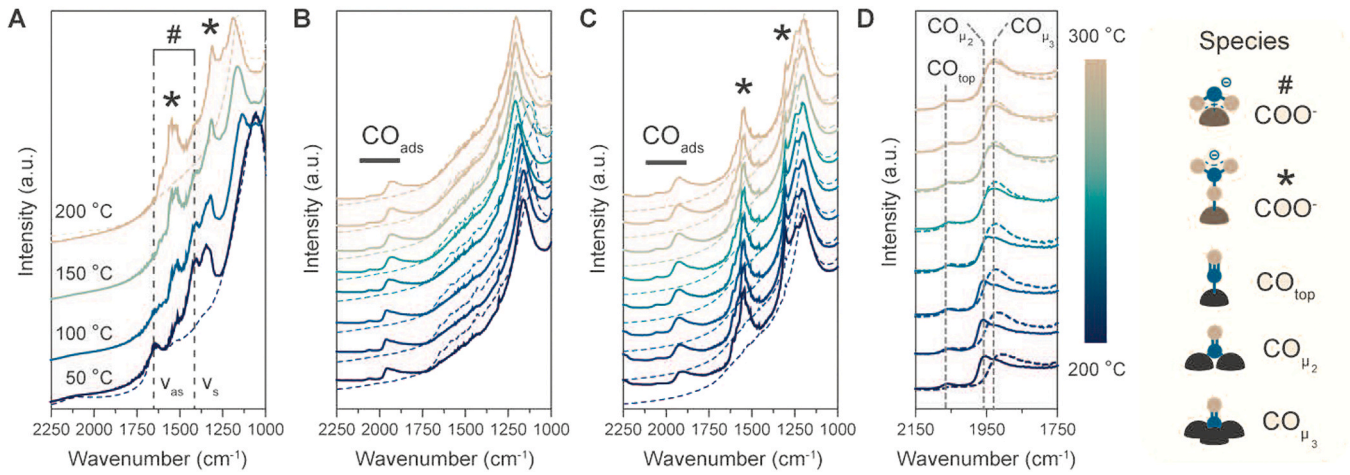

Fig. 8. (A) In situ Diffuse Reflectance Infrared Fourier Transform Spectroscopy (DRIFTS) spectra showing desorption of organic species during degassing under 50 mL/min N_2 flow in the temperature range 50–200 °C, over 3 Pd/Al_2O_3 500 °C (solid lines) and γ-Al_2O_3 calcined at 500 °C (dashed lines). (B,C) *operando* DRIFTS spectra during methane oxidation at 200–300 °C over 3Pd/Al_2O_3 250 °C (B) and 3 Pd/Al_2O_3 500 °C (C). Dashed lines correspond to γ-Al_2O_3 calcined at 250 °C (B) and 500 °C (C). (D) magnification of the CO_{ads} intermediate region showing evolution of PdO_x-CO interactions during catalysis. Solid lines: 3 Pd/Al_2O_3 250 °C; dashed lines: 3Pd/Al_2O_3 500 °C. Conditions (B-D): 10 mg of catalyst, 47.5 mL/min N_2, 0.5 mL/min CH_4, 2 mL/min O_2. The most relevant observed species are summarized in the panel on the right.

the observed activity trend: over the more active 3Pd/Al_2O_3 250 °C, OH groups at the Pd-Al_2O_3 interface can react (with other OH or H) and desorb as water, a step which can be rate limiting on Pd and Pt at the low temperatures used in this study [53]. On the other hand, on 3Pd/Al_2O_3 500 °C, the Pd-Al_2O_3 interface is dominated by strongly bound monodentate carbonates, slowing down H_2O desorption. Overall, these results provide evidence of the presence of different adsorbed species over the investigated catalysts under reaction conditions, and show a correlation exists between changes in adsorbates, Pd restructuring and catalytic activity.

4. Conclusions

This study describes the effects of calcination temperature on active phases, particle size, surface species and activity in methane combustion by Pd/ γ-Al_2O_3 catalysts. The Pd/Al_2O_3 catalysts were synthesized by the impregnation-vortexing method. Three catalysts containing 3.3 wt.% Pd/Al_2O_3 were calcined at 150 °C, 250 °C, and 500 °C. XPS confirmed the presence of PdO_x and PdO on the surface of both catalysts and conversion of some PdO_x to PdO and Pd^0 after reaction. HAADF-STEM images showed many small Pd particles (1–3 nm) on the support surface of the 3Pd/Al_2O_3 250 °C catalyst, while such small Pd particles were absent in the 3Pd/Al_2O_3 catalysts calcined at 150 and 500 °C. The growth of bigger Pd particles during the reaction is more pronounced in the catalysts calcined at lower temperatures. The results indicates varying degree of SMSI effects and evolution and restructuring of nanoparticles before and during the reaction in the three catalysts.

The light-off temperature for methane combustion was 250–255 °C for both catalysts and 100% methane combustion was achieved at 275 °C in 20 min with the 3Pd/Al_2O_3 250 °C catalyst under lean methane conditions. *Operando* DRIFTS experiments provided insights in temperature effects on Pd nanoparticles restructuring and Pd-alumina interfacial chemistry. The higher activity of 3Pd/Al_2O_3 250 °C was ascribed to the absence of dormant monodentate carbonate species (observed after high temperature calcination), which may hinder water desorption, a step which can be rate limiting on methane oxidation over Pd/Al_2O_3 at low temperatures. The evolution of adsorbed CO species further evidenced restructuring of the active 3Pd/Al_2O_3 250 °C during reaction, leading to the loss of μ_2-CO species.

To the best of our knowledge, the effects of calcination temperature on the properties, particle sizes and activities of Pd/Al_2O_3 catalysts have not been studied in similar details. This research study opens a possibility of altering catalytic properties and surfaces through calcination at different temperatures.

Funding

This research did not receive any specific grant from funding agencies in the public, commercial, or not-for-profit sectors.

CRediT authorship contribution statement

Domenica Fertal: Conceptualization, Methodology, Investigation, Visualization, Writing – original draft, Writing – review & editing. **Matteo Monai:** Conceptualization, Methodology, Investigation, Visualization, Writing – original draft, Writing – review & editing. **Laura Proaño:** Investigation, Visualization, Writing – review & editing. **Maxim Bukhovko:** Investigation, Visualization. **Jihyeon Park:** Investigation, Visualization. **Yong Ding:** Investigation, Visualization. **Bert M. Weckhuysen:** Investigation, Visualization, Writing – review & editing. **Anil Banerjee:** Conceptualization, Methodology, Visualization, Writing – original draft, Writing – review & editing, Supervision, Project management.

Declaration of Competing Interest

The authors declare that they have no known competing financial interests or personal relationships that could have appeared to influence the work reported in this paper.

Acknowledgment

Logistical support and small internal research grants provided by Columbus State University are acknowledged.

References

[1] M. Monai, T. Montini, R.J. Gorte, P. Fornasiero, Catalytic oxidation of methane: Pd and beyond, Eur. J. Inorg. Chem. 2018 (2018) 2884–2893, https://doi.org/10.1002/ejic.201800326.
[2] J. Chen, H. Arandiyan, X. Gao, J. Li, Recent advances in catalysts for methane combustion, Catal. Surv. Asia 19 (2015) 140–171, https://doi.org/10.1007/s10563-015-9191-5.

[3] L.M.T. Simplício, S.T. Brandão, E.A. Sales, L. Lietti, F. Bozon-Verduraz, Methane combustion over PdO-alumina catalysts: the effect of palladium precursors, Appl. Catal. B: Environ. 63 (2006) 9–14, https://doi.org/10.1016/j.apcatb.2005.08.009.

[4] J.J. Willis, A. Gallo, D. Sokaras, H. Aljama, S.H. Nowak, E.D. Goodman, L. Wu, C. J. Tassone, T.F. Jaramillo, F. Abild-Pedersen, M. Cargnello, Systematic structure-property relationship studies in palladium-catalyzed methane complete combustion, ACS Catal. 7 (2017) 7810–7821, https://doi.org/10.1021/acscatal.7b02414.

[5] A.C. Banerjee, J.M. McGuire, O. Lawnick, M.J. Bozack, Low-temperature activity and PdO-PdOx transition in methane combustion by a PdO-PdOx/γ-Al_2O_3 catalyst, Catalysts 8 (2018), https://doi.org/10.3390/catal8070266.

[6] K. Murata, Y. Mahara, J. Ohyama, Y. Yamamoto, S. Arai, A. Satsuma, The metal–support interaction concerning the particle size effect of Pd/Al_2O_3 on methane combustion, Angew. Chem. Int. Ed. 56 (2017) 15993–15997, https://doi.org/10.1002/anie.201709124.

[7] J. Chen, J. Zhong, Y. Wu, W. Hu, P. Qu, X. Xiao, G. Zhang, X. Liu, Y. Jiao, L. Zhong, Y. Chen, Particle size effects in stoichiometric methane combustion: structure-activity relationship of Pd catalyst supported on gamma-alumina, ACS Catal. 10 (2020) 10339–10349, https://doi.org/10.1021/acscatal.0c03111.

[8] S. Colussi, A. Trovarelli, C. Cristiani, L. Lietti, G. Groppi, The influence of ceria and other rare earth promoters on palladium-based methane combustion catalysts, Catal. Today 180 (2012) 124–130, https://doi.org/10.1016/j.cattod.2011.03.021.

[9] J. Ma, Y. Lou, Y. Cai, Z. Zhao, L. Wang, W. Zhan, Y. Guo, Y. Guo, The relationship between the chemical state of Pd species and the catalytic activity for methane combustion on Pd/CeO_2, Catal. Sci. Technol. 8 (2018) 2567–2577, https://doi.org/10.1039/c8cy00208h.

[10] R. Ramírez-López, I. Elizalde-Martinez, L. Balderas-Tapia, Complete catalytic oxidation of methane over Pd/CeO_2-Al_2O_3: the influence of different ceria loading, Catal. Today 150 (2010) 358–362, https://doi.org/10.1016/j.cattod.2009.10.007.

[11] M. Cargnello, J.J.D. Jaén, J.C.H. Garrido, K. Bakhmutsky, T. Montini, J.J. C. Gámez, R.J. Gorte, P. Fornasiero, Exceptional activity for methane combustion over modular Pd@CeO_2 subunits on functionalized Al_2O_3, Science 337 (2012) 713–718, https://doi.org/10.1126/science.1222887.

[12] X. Liu, J. Liu, F. Geng, Z. Li, P. Li, W. Gong, Synthesis and properties of PdO/CeO_2-Al_2O_3 catalysts for methane combustion, Front. Chem. Sci. Eng. 6 (2012) 34–37, https://doi.org/10.1007/s11705-011-1163-3.

[13] D. Fertal, M. Bukhovko, Y. Ding, B. Mehmet, A. Banerjee, Particle size and PdO–support interactions in PdO/CeO_2-γ Al_2O_3 catalysts and effect on methane combustion, Catalysts 10 (2020) 976, https://doi.org/10.3390/catal10090976.

[14] M. Ahmadi, H. Mistry, B. Roldan Cuenya, Tailoring the catalytic properties of metal nanoparticles via support interactions, J. Phys. Chem. Lett. 7 (2016) 3519–3533, https://doi.org/10.1021/acs.jpclett.6b01198.

[15] L. Liu, A. Corma, Metal catalysts for heterogeneous catalysis: from single atoms to nanoclusters and nanoparticles, Chem. Rev. 118 (2018) 4981–5079, https://doi.org/10.1021/acs.chemrev.7b00776.

[16] L. Piccolo, Restructuring effects of the chemical environment in metal nanocatalysis and single-atom catalysis, Catal. Today 373 (2021) 80–97, https://doi.org/10.1016/j.cattod.2020.03.052.

[17] P. Gélin, M. Primet, Complete oxidation of methane at low temperature over noble metal based catalysts: a review, Appl. Catal. B: Environ. 39 (2002) 1–37, https://doi.org/10.1016/S0926-3373(02)00076-0.

[18] F. Huang, J. Chen, W. Hu, G. Li, Y. Wu, S. Yuan, L. Zhong, Y. Chen, Pd or PdO: catalytic active site of methane oxidation operated close to stoichiometric air-to-fuel for natural gas vehicles, Appl. Catal. B: Environ. 219 (2017) 73–81, https://doi.org/10.1016/j.apcatb.2017.07.037.

[19] J. Nilsson, P.A. Carlsson, N.M. Martin, E.C. Adams, G. Agostini, H. Grönbeck, M. Skoglundh, Methane oxidation over Pd/Al_2O_3 under rich/lean cycling followed by operando XAFS and modulation excitation spectroscopy, J. Catal. 356 (2017) 237–245, https://doi.org/10.1016/j.jcat.2017.10.018.

[20] N. Sadokhina, F. Ghasempour, X. Auvray, G. Smedler, U. Nylén, M. Olofsson, L. Olsson, An experimental and kinetic modelling study for methane oxidation over Pd-based catalyst: inhibition by water, Catal. Lett. 147 (2017) 2360–2371, https://doi.org/10.1007/s10562-017-2133-2.

[21] V.Y. Bychkov, Y.P. Tyulenin, A.Y. Gorenberg, S. Sokolov, V.N. Korchak, Evolution of Pd catalyst structure and activity during catalytic oxidation of methane and ethane, Appl. Catal. A: Gen. 485 (2014) 1–9, https://doi.org/10.1016/j.apcata.2014.07.028.

[22] K. Murata, D. Kosuge, J. Ohyama, Y. Mahara, Y. Yamamoto, S. Arai, A. Satsuma, Exploiting metal-support interactions to tune the redox properties of supported Pd catalysts for methane combustion, ACS Catal. 10 (2020) 1381–1387, https://doi.org/10.1021/acscatal.9b04524.

[23] A. Baylet, P. Marécot, D. Duprez, P. Castellazzi, G. Groppi, P. Forzatti, In situ Raman and in situ XRD analysis of PdO reduction and Pd^0 oxidation supported on γ-Al_2O_3 catalyst under different atmospheres, Phys. Chem. Chem. Phys. 13 (2011) 4607–4613, https://doi.org/10.1039/c0cp01331e.

[24] J.B. Miller, M. Malatpure, Pd catalysts for total oxidation of methane: support effects, Appl. Catal. A: Gen. 495 (2015) 54–62, https://doi.org/10.1016/j.apcata.2015.01.044.

[25] N.M. Kinnunen, M. Suvanto, M.A. Moreno, A. Savimäki, K. Kallinen, T.J. J. Kinnunen, T.A. Pakkanen, Methane oxidation on alumina supported palladium catalysts: effect of Pd precursor and solvent, Appl. Catal. A: Gen. 370 (2009) 78–87, https://doi.org/10.1016/j.apcata.2009.09.018.

[26] W.R. Schwartz, L.D. Pfefferle, Combustion of methane over palladium-based catalysts: support interactions, J. Phys. Chem. C 116 (2012) 8571–8578, https://doi.org/10.1021/jp2119668.

[27] A.Y. Stakheev, A.M. Batkin, N.S. Teleguina, G.O. Bragina, V.I. Zaikovsky, I. P. Prosvirin, A.K. Khudorozhkov, V.I. Bukhtiyarov, Particle size effect on CH_4 oxidation over noble metals: comparison of Pt and Pd catalysts, Top. Catal. 56 (2013) 306–310, https://doi.org/10.1007/s11244-013-9971-y.

[28] K. Murata, J. Ohyama, Y. Yamamoto, S. Arai, A. Satsuma, Methane combustion over Pd/Al_2O_3 catalysts in the presence of water: effects of Pd particle size and alumina crystalline phase, ACS Catal. 10 (2020) 8149–8156, https://doi.org/10.1021/acscatal.0c02050.

[29] T.R. Baldwin, R. Burch, Catalytic combustion of methane over supported palladium catalysts. II. Support and possible morphological effects, Appl. Catal. 66 (1990) 359–381, https://doi.org/10.1016/S0166-9834(00)81649-8.

[30] G. Zhu, J. Han, D.Y. Zemlyanov, F.H. Ribeiro, The turnover rate for the catalytic combustion of methane over palladium is not sensitive to the structure of the catalyst, J. Am. Chem. Soc. 126 (2004) 9896–9897, https://doi.org/10.1021/ja049406s.

[31] J. Nilsson, P.A. Carlsson, S. Fouladvand, N.M. Martin, J. Gustafson, M.A. Newton, E. Lundgren, H. Grönbeck, M. Skoglundh, Chemistry of supported palladium nanoparticles during methane oxidation, ACS Catal. 5 (2015) 2481–2489, https://doi.org/10.1021/cs502036d.

[32] Z. Boukha, A. Choya, M. Cortés-Reyes, B. de Rivas, L.J. Alemany, J.R. González-Velasco, J.I. Gutiérrez-Ortiz, R. López-Fonseca, Influence of the calcination temperature on the activity of hydroxyapatite-supported palladium catalyst in the methane oxidation reaction, Appl. Catal. B: Environ. 277 (2020), 119280, https://doi.org/10.1016/j.apcatb.2020.119280.

[33] J.J. Lovón-Quintana, J.B.O. Santos, A.S.P. Lovón, N. La-salvia, G.P. Valenc, Low-temperature oxidation of methane on Pd-Sn/ZrO_2 catalysts, J. Mol. Catal. A: Chem. 411 (2016) 117–127, https://doi.org/10.1016/j.molcata.2015.08.001.

[34] A. Eyssler, A. Winkler, P. Mandaliev, P. Hug, A. Weidenkaff, D. Ferri, Influence of thermally induced structural changes of 2wt.% Pd/$LaFeO_3$ on methane combustion activity, Appl. Catal. B: Environ. 106 (2011) 494–502, https://doi.org/10.1016/j.apcatb.2011.06.008.

[35] R. Gholami, K.J. Smith, Activity of PdO/SiO_2 catalysts for CH_4 oxidation following thermal treatments, Appl. Catal. B: Environmen. 168–169 (2015) 156–163, https://doi.org/10.1016/j.apcatb.2014.12.037.

[36] D. Domingos, L.M.T.S. Rodrigues, S.T. Brandão, M.D.G.C. Da Rocha, R. Frety, Palladium-supported catalysts in methane combustion. Comparison of alumina and Zirconia supports, Quimica Nova 35 (2012) 1118–1122, https://doi.org/10.1590/S0100-40422012000600009.

[37] A.C. Banerjee, K.W. Golub, M.A. Hakim, M.Z. Billor, Comparative study of the characteristics and activities of Pd/ -Al_2O_3 catalysts prepared by vortex and incipient wetness methods,, Catalysts 9 (2019), https://doi.org/10.3390/catal9040336.

[38] T.P. Sulmonetti, S.H. Pang, M.T. Claure, S. Lee, D.A. Cullen, P.K. Agrawal, C. W. Jones, Vapor phase hydrogenation of furfural over nickel mixed metal oxide catalysts derived from layered double hydroxides, Appl. Catal. A: Gen. 517 (2016) 187–195, https://doi.org/10.1016/j.apcata.2016.03.005.

[39] Y. Ding, Y. Chen, K.C. Pradel, W. Zhang, M. Liu, Z.L. Wang, Domain structures and Pr co antisite point defects in double-perovskite, Ultramicroscopy 193 (2018) 64–70, https://doi.org/10.1016/j.ultramic.2018.06.008.

[40] A.R. Puigdollers, P. Schlexer, S. Tosoni, G. Pacchioni, Increasing oxide reducibility: the role of metal/oxide interfaces in the formation of oxygen vacancies, ACS Catal. 7 (2017) 6493–6513, https://doi.org/10.1021/acscatal.7b01913.

[41] R.J. Farrauto, M.C. Hobson, T. Kennelly, E.M. Waterman, Catalytic chemistry of supported palladium for combustion of methane, Appl. Catal. A Gen. 81 (1992) 227–237, https://doi.org/10.1016/0926-860X(92)80095-T.

[42] B. Van Devener, S.L. Anderson, T. Shimizu, H. Wang, J. Nabity, J. Engel, J. Yu, D. Wickham, S. Williams, In situ generation of Pd/PdO nanoparticle methane combustion catalyst: Correlation of particle surface chemistry with ignition, J. Phys. Chem. C 113 (2009) 20632–20639, https://doi.org/10.1021/jp904317y.

[43] J.M. Giraudon, A. Elhachimi, G. Leclercq, Catalytic oxidation of chlorobenzene over Pd/perovskites, Appl. Catal. B: Environ. 84 (2008) 251–261, https://doi.org/10.1016/j.apcatb.2008.04.023.

[44] N. Yang, J. Liu, Y. Sun, Y. Zhu, Correction: Au@PdO_x with a PdO_x-rich shell and Au-rich core embedded in Co_3O_4 nanorods for catalytic combustion of methane, Nanoscale 11 (2019) 4108–4109, https://doi.org/10.1039/c9nr90025j.

[45] F. Huang, J. Chen, W. Hu, G. Li, Y. Wu, S. Yuan, L. Zhong, Y. Chen, Pd or PdO: catalytic active site of methane oxidation operated close to stoichiometric air-to-fuel for natural gas vehicles, Appl. Catal. B: Environ. 219 (2017) 73–81, https://doi.org/10.1016/j.apcatb.2017.07.037.

[46] M. Schmal, M.M.V.M. Souza, V.V. Alegre, M.A.P. da Silva, D.V. César, C.A.C. Perez, Methane oxidation - effect of support, precursor and pretreatment conditions-in situ reaction XPS and DRIFT, Catal. Today 118 (2006) 392–401, https://doi.org/10.1016/j.cattod.2006.07.026.

[47] J.J. Willis, E.D. Goodman, L. Wu, A.R. Riscoe, P. Martins, C.J. Tassone, M. Cargnello, Systematic identification of promoters for methane oxidation catalysts using size- and composition-controlled Pd-Based bimetallic nanocrystals, J. Am. Chem. Soc. 139 (2017) 11989–11997, https://doi.org/10.1021/jacs.7b06260.

[48] I.E. Wachs, Molecular Spectroscopy of Oxide Catalyst Surfaces By Anatoli Davydov (University of Alberta and Syntroleum Corporation, Tulsa, OK), John Wiley & Sons, Inc, Hoboken, 2003.

[49] J.B. Peri, R.B. Hannan, Surface hydroxyl groups on γ-alumina, J. Phys. Chem. 64 (1960) 1526–1530, https://doi.org/10.1021/j100839a044.

[50] A.M. McCullagh, R. Warringham, C.G.A. Morisse, L.F. Gilpin, C. Brennan, C. J. Mitchell, D.A. Lennon, A comparison of experimental procedures for the application of infrared spectroscopy to probe the surface morphology of an

alumina-supported palladium catalyst!Abstract, No. 0123456789, Top. Catal. (2021), https://doi.org/10.1007/s11244-021-01435-y.
[51] G. Spezzati, Y. Su, J.P. Hofmann, A.D. Benavidez, A.T. DeLaRiva, J. McCabe, A. K. Datye, E.J.M. Hensen, Atomically dispersed Pd–O species on CeO_2 (111) as highly active sites for low-temperature CO oxidation, ACS Catal. 7 (2017) 6887–6891, https://doi.org/10.1021/acscatal.7b02001.
[52] E.J. Jang, J. Lee, D.G. Oh, J.H. Kwak, CH_4 oxidation activity in Pd and Pt–Pd bimetallic catalysts: correlation with surface PdOx quantified from the DRIFTS study, ACS Catal. 11 (2021) 5894–5905, https://doi.org/10.1021/acscatal.1c00156.
[53] A. Trinchero, A. Hellman, H. Grönbeck, Methane oxidation over Pd and Pt studied by DFT and kinetic modeling, Surf. Sci. 616 (2013) 206–213, https://doi.org/10.1016/j.susc.2013.06.014.